

# Insights into the Electronic Structure of Ceramics through Quantitative Analysis of Valence Electron Energy-loss Spectroscopy

Harald Müllejans<sup>1,2\*</sup> and Roger H. French<sup>1,3</sup>

<sup>1</sup>Max-Planck-Institut für Metallforschung, Seestraße 92, D-70174 Stuttgart, Germany

<sup>2</sup>Institute for Advanced Materials, Joint Research Centre, European Commission, P.O. Box 2, NL-1755 ZG Petten, The Netherlands

<sup>3</sup>DuPont Central Research, E356-384 Experimental Station, Wilmington, DE 19880

**Abstract:** Valence electron energy-loss (VEEL) spectroscopy was performed on six ceramic materials in a dedicated scanning transmission electron microscope (STEM). Quantitative analysis of these data is described yielding access to the complex optical properties and the electronic structure of the materials. Comparisons are made on the basis of the interband transition strength describing transitions between occupied states in the valence band and empty states in the conduction band. This proves that the quantitative analysis of VEEL data is a competitive and complementary method to be considered when investigating the electronic structure of materials. Possibilities for improvement and extension of the analysis are discussed extensively.

**Key words:** scanning transmission electron microscope, valence electron energy-loss spectroscopy, ceramics, electronic structure, optical properties, data analysis, interband transition strength, quantitative analysis

## INTRODUCTION

The electronic structure of ceramic materials is increasingly of interest because of the use of ceramic materials in optical, electronic, and structural applications. There is also extensive effort in determining optical properties and electronic structure from either *ab initio* or semi-empirical theory (Ching, 1990; Xu and Ching, 1991, 1993) or by experiment, notably vacuum ultraviolet (VUV) spectroscopy (French, 1990a, b; French et al., 1994). This has shown that the electronic structure can be derived from any optical property as long as both the real and imaginary parts of the complex optical property are known (French, 1990a). In

practice, it requires only the knowledge of the real *or* imaginary part of any of the complex optical properties (over all energies) since its complex conjugate can be determined using Kramers-Kronig (KK) analysis (Kramers, 1927; Kronig, 1926; Gorter and Kronig, 1936).

It is well known that electron energy-loss (EEL) spectroscopy in the transmission electron microscope (TEM) provides the energy-loss function  $ELF = -\text{Im}[1/\hat{\epsilon}]$  where  $\hat{\epsilon}$  is the complex dielectric function. Archie Howie and his coworkers have been the most eminent group in understanding the valence part of the EEL spectrum from dielectric theory (Ritchie and Howie, 1977). In most cases, the valence electron energy-loss (VEEL) spectra have been calculated from literature values of the dielectric function of the materials and including the geometry of the experiment, i.e., the presence of surfaces (Walls, 1987; Walls and Howie, 1989) and interfaces (Howie and Milne, 1985), holes

Received November 9, 1999; accepted December 20, 1999.

\*Corresponding author, at the Institute for Advanced Materials, Joint Research Centre, European Commission, P.O. Box 2, NL-1755 ZG Petten, The Netherlands.

(Walsh, 1989), small particles (Echenique et al., 1987), or composite media (Howie and Walsh, 1991). The results compared favorably with experiment.

There has been less effort to determine the dielectric function and optical properties (Daniels et al., 1970; Fink, 1989; Ryen et al., 1999) or electronic structure (Gautier et al., 1987) from VEEL spectroscopy. However, the well-known theory of VEEL (Egerton, 1996) provides us with the route to follow. This has not been explored widely because the link from dielectric properties to electronic structure has not been realized despite of Wooten's book (1972). Also many practical problems are encountered when performing the analysis. However, the attraction of having a relatively simple and straightforward method available [VEEL spectroscopy in a dedicated scanning transmission electron microscope (STEM)] paired with the high spatial resolution available in electron microscopy has led us to pursue this avenue with vigor. In the development, we have made extensive use of results from VUV spectroscopy (Müllejjans et al., 1993, 1994; Müllejjans and French, 1996; French et al., 1998a). However, now we have reached a point where the analysis of VEEL data can be performed with enough confidence so that reference data from other sources are no longer essential. An account of these methods (Dorneich et al., 1998) for interpretation of optical properties (French et al., 1998a), electronic structure (Jones et al., 1999), changes in bonding at grain boundaries (Müllejjans and French, 1996), and the calculation of intergranular forces in silicon nitride (French et al., 1995b; French et al., 1998b) has been given elsewhere. In this contribution, we therefore concentrate on the current method of analyzing VEEL data fully quantitatively yielding reliable results for six different ceramic materials, some of which have not been investigated with respect to electronic structure before. The discussion is directed to the current challenges in the analysis and the future possibilities in this field.

## MATERIALS AND METHODS

### Hardware and Data Acquisition

Six different ceramic materials were investigated: two phases of alumina ( $\alpha$ -Al<sub>2</sub>O<sub>3</sub> and  $\gamma$ -Al<sub>2</sub>O<sub>3</sub>), Magnesia (MgO), magnesium aluminate spinel (MgAl<sub>2</sub>O<sub>4</sub>), calcium-hexa-aluminate (CaO(Al<sub>2</sub>O<sub>3</sub>)<sub>6</sub>), and silicon nitride ( $\beta$ -Si<sub>3</sub>N<sub>4</sub>). The sample and TEM specimen preparation for the two alumina phases and the silicon nitride has been de-

scribed elsewhere (Levin et al., 1997; French et al., 1998a, b). Magnesia smoke cubes were obtained by burning pure magnesium in air and moving a 3 mm-diameter TEM specimen grid with holy carbon film once through the white smoke. This yielded perfectly cubic magnesia cubes with typical edge lengths between 10 and 100 nm. The magnesium aluminate spinel was from a single crystal with stoichiometric composition (Commercial Crystal Laboratories, Naples, FL). Details about the material and the TEM specimen preparation have been published elsewhere (Schweinfest et al., 1999). The calcium-hexa-aluminate was synthesized from high purity CaCO<sub>3</sub> (Merck) and Al<sub>2</sub>O<sub>3</sub> (Alcoa, Pittsburgh, PA) by solid state reaction. The starting mixture of both powders, weighed in correct proportion, was wet milled and pressed into pellets which were calcined two times at 1200°C for 16 hr and sintered at 1550°C for 12 hr. The calcium-hexa-aluminate formation was confirmed by X-ray powder diffraction. A 3 mm-diameter disc was cut from a pellet, mechanical thinned, dimpled, and ion beam thinned until perforation. Carbon coating was not applied to the specimens, as specimen charging during the experiments was not observed.

All TEM specimens were examined in vacuum generators (VG; Fisons Instruments, East Grinstead, UK) HB501 UX dedicated STEM equipped with a Gatan 666 parallel electron energy-loss spectrometer (PEELS). The data acquisition of the PEELS had been upgraded by a photodiode with less dark current and noise (as described in Colliex et al., 1994). The signal output from the electronics for spectrum acquisition was processed by simple electronics to give logic (TTL) signals with two alternating lengths. The first is equal to the full acquisition length set in the El/P software (Gatan, 1994) (typically 1 sec) and the second is much shorter (adjustable between 2 and 25 msec) (Müllejjans et al., 1997; French et al., 1998b). This logic signal was connected to the beam blanker on the STEM, yielding an illumination time of the specimen alternating between typically 1 sec and 20 msec. This allows the acquisition of two consecutive spectra by the El/P software without changing the integration time of the photodiode array but with largely varying intensity. Effectively, the dynamic range of the data acquisition is enlarged.

It is also possible to acquire a series of spectra in this mode with the beam stepping after every second spectrum using a Gatan Digiscan module controlling the scanning of the electron beam and some specially written software. In this mode, two spectra are acquired for each pixel in a line profile or image, one with low beam intensity (short illu-

mination time) and one with higher beam intensity (longer illumination time). This same software was also used to improve the signal-to-noise ratio in the spectra by acquiring a series without stepping the beam (i.e., Digiscan disconnected and scan control from the microscope console, typically reduced area scan at a magnification of 10M corresponding to an illuminated area of  $3 \times 4 \text{ nm}^2$ ). This is not a limitation for the materials investigated here since the crystallite size was much larger and the thickness variations over this area are negligible.

In practice integration time of the photodiode array (corresponding to the long illumination time) was set so that the maximum of the plasmon peak in the VEEL spectrum was below saturation (ca. 16,000 photodiode counts) but well above 10,000 counts. Then, the short illumination time was adjusted until the maximum of the zero loss peak was in the same intensity range. The two spectra are labeled plasmon and zero loss optimized, respectively. The plasmon optimized is saturated at the zero loss peak, but has a higher signal-to-noise ratio for all other energy losses. The data were acquired with a custom function written to run under El/P on the Macintosh computer controlling the PEELS data acquisition system (French et al., 1998b).

Spectra were acquired at 100 keV primary energy, with the convergence semi-angle of 10 mrad and a collection semi-angle of 13 mrad. The spectrometer dispersion was typically 0.1 eV per channel yielding a total spectrum width of 100 eV. Typical energy resolution was 0.7 eV. In some cases, the spectra were acquired manually, i.e., changing the readout time of the photodiode array in the El/P software and acquiring spectra (multiple readouts) for short and long times. In this mode, it was also possible (and done in some cases) to acquire an additional spectrum at higher energy losses to cover low lying absorption edges (typical shift of 50 eV to catch the Al L-edge).

All spectra were corrected for dark current (separately acquired with identical photodiode integration time and number of multiple readouts, but without electron beam) and gain variations. These corrections are mathematically trivial and were easily implemented on the Macintosh computer. The following steps of analysis however are mathematically sophisticated and require specialized custom-written software. Therefore, the spectra were transferred to a PC running under Windows and analyzed with electronic structure tools (Spectrum Square Associates, 1998), an extensive analysis package developed within Grams (Galactic Industries, 1996).

## Software and Data Analysis

The data analysis consists of a number of steps, which will be outlined below. Special attention will be given to points improved since the last extensive report (Dorneich et al., 1998). First, the two spectra (plasmon and zero loss optimized) were joined (spliced together) to give a single spectrum with extended dynamic range. This was achieved by calculating a scaling factor between both spectra from the regions of unsaturated intensity on both sides of the zero loss peak. The saturated region in the plasmon optimized spectrum was then replaced with the scaled intensity of the zero loss optimized spectrum. Because of instabilities of the system (microscope and spectrometer), small energy shifts might have occurred between the acquisition of the two spectra. The shift was calculated by the software and then corrected allowing shifts between both spectra in fractions of a 0.1 eV channel.

The next step was the removal of multiple scattering contributions and the zero loss peak to arrive at the  $ELF = -\text{Im}[1/\hat{\epsilon}]$ . For the removal of multiple scattering, primarily occurring in the spectrum at energy losses above the plasmon energy, the total integrated intensity of the zero loss is important but its exact shape is not. This part of the analysis is therefore not sensitive to assumptions about the high energy wing of the zero loss peak extending under the measured spectrum, because this wing contains only marginal intensity. However, the reliable and accurate removal of the zero loss peak was crucial for intensities at energy losses just above the band gap of the ceramic materials. An asymmetric Pearson VII function (see details in Dorneich et al., 1998) was fitted into the zero loss peak for all energy losses (starting at nominally negative energy losses) up to an energy loss for which no transitions are expected (set by the operator smaller than the band gap of the ceramic) and then extrapolated to higher energies. The removal of the plural scattering is based on a Fourier-log deconvolution method (Egerton, 1996). A correction for the finite collection angle was not applied.

Up to this point, all intensities are on an arbitrary scale. The absolute scaling of the data was obtained by the index of refraction sum rule scaling (Egerton, 1996). The index of refraction in the visible was obtained from data sources (Lide, 1994). Furthermore, the experimentally measured data was extended to 1000 eV by adding a high energy-loss wing. This wing was modeled as  $A^*E^{-4}$  ( $A$  is a constant and  $E$  is the energy loss) and fit to the last 5–10 eV of the spectrum.

KK-analysis based on fast Fourier transformation (FFT) (Johnson, 1975; Bortz and French, 1989) then yielded  $\text{Re}[1/\hat{\epsilon}]$ , the complex conjugate of the *ELF*. All other (complex) optical properties were calculated algebraically from knowledge of the real and imaginary part of the *ELF*. This provides, for example, the complex dielectric function  $\hat{\epsilon} = \epsilon_1 + i\epsilon_2$ , the complex index of refraction  $\hat{n} = n + ik$ , where  $n$  is the refractive index and  $k$  the extinction coefficient, the surface energy-loss function  $-\text{Im}[1/(\hat{\epsilon} + 1)]$ , the reflectivity  $R$  and the reflected phase  $\theta$ , the optical conductivity  $\hat{\sigma} = \sigma_1 + i\sigma_2$ , the absorption coefficient  $\alpha = 4\pi k/\lambda$ , and the complex interband transition strength  $\hat{J}_{cv}$ , all as function of energy  $E$ . The interband transition strength  $\hat{J}_{cv}$ , defined in equation (1), is directly related to the electronic structure of the material:

$$\hat{J}_{cv}(E) = J_{cv1} + i J_{cv2} = \frac{m_0^2}{e^2 \hbar^2} \frac{E^2}{8\pi^2} (\epsilon_2(E) + i\epsilon_1(E)) \quad (1)$$

where  $m_0$  is the electron mass and  $e$  its charge. The real part of the interband transition strength gives the probability of a transition between a filled state in the valence band and an empty state in the conduction band as a function of transition energy. It was chosen here for comparing the results obtained from the different ceramic materials. It can also serve as a common basis for comparing results from different experimental techniques (French et al., 1998a) or with respect to theoretical calculations.

The effective number of electrons  $n_{\text{eff}}$  contributing to transitions up to energy  $E$  can be calculated using the oscillator strength or  $f$  sum rule (Smith, 1985; Egerton, 1996), shown in equation (2), evaluated on  $J_{cv1}$ :

$$n_{\text{eff}}(E)|_{J_{cv1}} = \frac{4v_f}{m_0} \int_0^E \frac{J_{cv1}(E')}{E'} dE' \quad (2)$$

where  $v_f$  is the volume of material corresponding to one chemical formula unit.

## RESULTS

The spliced energy-loss spectra, the zero loss function, and the single scattering distribution for the six ceramic materials are collected in Figure 1. The real part of the interband transition strength is presented in Figure 2.

The parameters used in the calculation of the  $f$  sum rule [equation (2)] are given in Table 1, which also contains the

number of electrons per formula unit and the effective number of electrons for transitions up to 80 eV, the results are presented in Figure 3.

## DISCUSSION

### Interband Transitions and Electronic Structure

A comparison of the interband transition strength for the two different phases of alumina shows marked differences. The peak at 14 eV has less intensity for  $\gamma$ -alumina, the peak at 19 eV likewise in particular on the high energy side. Two peaks at 32 and 46 eV are present for  $\alpha$ -alumina but only one at 40 eV for  $\gamma$ -alumina. Similar features are repeated in the transition from the Al L-shell above 77 eV (Fig. 2a). Thus the electronic structure of different phases of the same material varies. This is not surprising since the crystal lattice is different (symmetry, lattice constant). However, now we can address these differences in detail. We might even be able to identify certain phases by their electronic structure similar to what has been proposed and demonstrated for ELNES (Craven and MacKenzie, 1999). This demonstrates that changes in electronic structure between two materials can be determined accurately.

By comparing the results for calcium-hexa-aluminate (Fig. 2a) with those of the alumina phases, it is obvious that the pure alumina exhibits more and sharper features. The structure above 77 eV of calcium-hexa-aluminate bears some resemblance to the structure for  $\gamma$ -alumina, however, the valence to conduction band transition does not, with the absence of the peak at 14 eV for calcium-hexa-aluminate.

A similar effect is seen when considering the results for magnesium aluminate spinel (Fig. 2b). Here one can see that the electronic structure of a chemical compound is far different from those of its two components (magnesia and alumina). The electronic structure is therefore far from being a simple mixture, as has also been discussed by Mo and Ching (1996) in their band structure article on magnesium aluminate spinel. VEEL spectroscopy now provides us with a method to study the electronic structure and its changes directly.

The sum rule [equation (2)] for the materials (Fig. 3, Table 1) provides a comparison between the different ceramic materials as well as a convenient check on the plausibility of the data (Shiles et al., 1980). The effective number of electrons is calculated per (chemical) formula unit and it

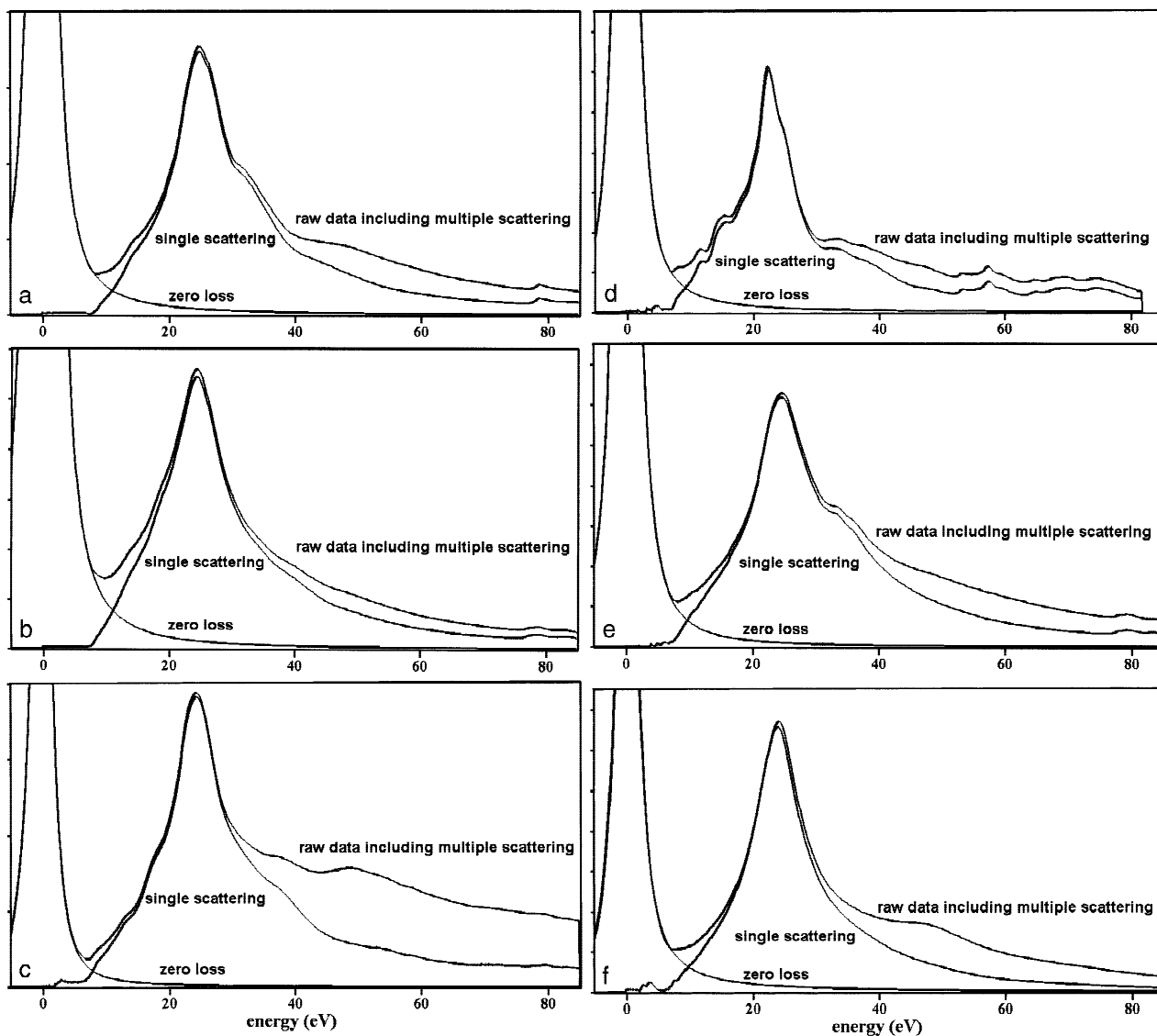


**Figure 1.** Valence electron energy-loss (VEEL) spectra of ceramics; all intensities are in arbitrary units: (a)  $\alpha$ - $\text{Al}_2\text{O}_3$ ; (b)  $\gamma$ - $\text{Al}_2\text{O}_3$ ; (c)  $\text{MgAl}_2\text{O}_4$ ; (d)  $\text{MgO}$ ; (e)  $\text{CaO}(\text{Al}_2\text{O}_3)_6$ ; and (f)  $\beta$ - $\text{Si}_3\text{N}_4$ .

should be compared with the expected number of valence electrons per formula unit (Table 1). Magnesia has 5.2 electrons contributing to transitions up to 50 eV (just before the Mg L-edge). This compares to the eight valence electrons per  $\text{MgO}$  molecule. However, it is not to be expected that all transitions are exhausted at 50 eV.

For the alumina phases 20.5 ( $\gamma$ - $\text{Al}_2\text{O}_3$ ) and 22 ( $\alpha$ - $\text{Al}_2\text{O}_3$ ), electrons are reached by 80 eV as opposed to the total of 24 valence electrons which are expected to participate in the transitions. The Al L-edge plays a minor role as it starts just before 80 eV. Thus, for alumina, almost all transitions from the valence band are exhausted by 80 eV transition energy. There is no obvious reason why the values

for  $\gamma$ - $\text{Al}_2\text{O}_3$  are always lower than those for  $\alpha$ - $\text{Al}_2\text{O}_3$ . Silicon-nitride reaches about 27.3 effective electrons out of 32, showing that most transitions are exhausted but some remain for higher transition energies. For spinel, 21.5 out of 32 electrons are reached by 50 eV before the Mg L-edge. Calcium-hexa-aluminate has a much larger number of valence electrons per formula unit (152) and  $n_{\text{eff}} = 117$  at 80 eV. The highest percentage of transitions is exhausted for the two alumina phases, whereas for the two materials containing Mg it is lowest (Table 1). The remaining two materials have values between these two extremes.

Ideally, the effective number of electrons should saturate just before the onset of new transitions (e.g., an ab-

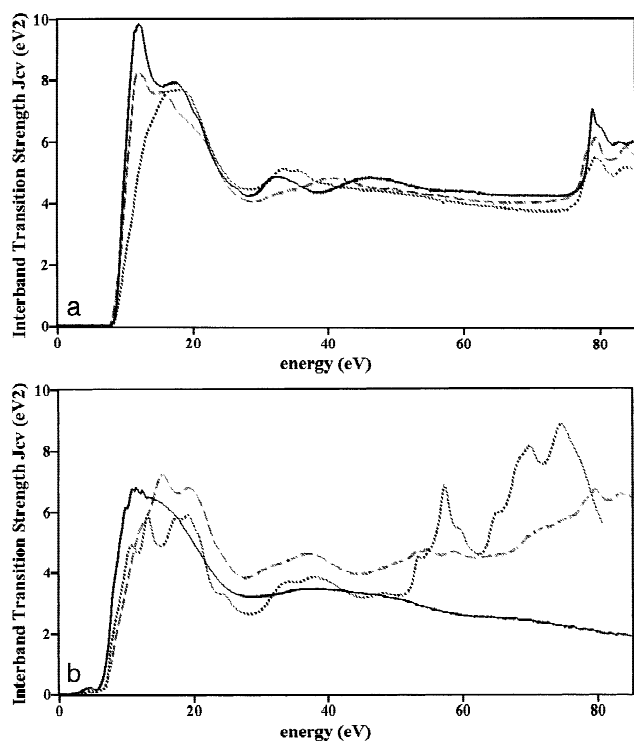


**Figure 2.** Real part of the interband transition strength  $J_{CV}$  from data of Figure 1: (a)  $\alpha$ - $\text{Al}_2\text{O}_3$  (continuous line),  $\gamma$ - $\text{Al}_2\text{O}_3$  (dashed line), and  $\text{CaO}(\text{Al}_2\text{O}_3)_6$  (dotted line); (b)  $\beta$ - $\text{Si}_3\text{N}_4$  (continuous line),  $\text{MgAl}_2\text{O}_4$  (dashed line), and  $\text{MgO}$  (dotted line).

sorption edge). However, this behavior is rarely observed in practice (Shiles et al., 1980; Smith, 1985). There is also some discussion of redistribution of oscillator strength between different types of transitions (Shiles et al., 1980), although these effects are thought to be minor corrections. The oscillator strength sum rule only applies strictly to the sum of all transitions evaluated over all energies. For the ceramic materials investigated here, the interband transitions are never exhausted before the onset of the low lying inner shell absorption edges, which explains the values (in percent) reached for the effective number of electrons. In conclusion, the sum rule evaluated here does not give any indication of inconsistencies in the data.

### Data Analysis and EEL Techniques

The extension of the data by a high energy wing is necessary for the KK analysis. As it was found that the data analysis is not sensitive to the details of this spectral region, a simple mathematical form was chosen rather than measuring the EEL spectrum. However, this would be necessary if information in this energy range is required.

The analysis of the spectra was possible because a band gap of several eV is present in these ceramic materials. Therefore, no transitions are assumed up to the band gap energy and the line shape for the zero loss peak can be fitted and extrapolated to higher energies. This limits the analysis to non-metallic materials, exhibiting non-zero band gap energies. For semiconductors, the small band gap leaves only a limited fitting range yielding numerical problems of accuracy. We are currently developing methods to perform the analysis on metallic materials, using data from ellipsometry in the visible, extrapolating the energy-loss function to 0 eV, and thereby removing the need for the no transition energy (Jones et al., 1999).

It is well known that there might be intensities in the band gap, for gap states (induced by specimen surfaces) as well as from Cerenkov radiation and “Bremsstrahlung” (Egerton, 1996). However, they are not of interest here and are eliminated to first order by the procedure chosen. The residual intensities visible in the band gap region for some of the results (Fig. 1) are artifacts due to imperfect fitting of the Pearson VII function to the zero loss peak. They are also disregarded in the further analysis.

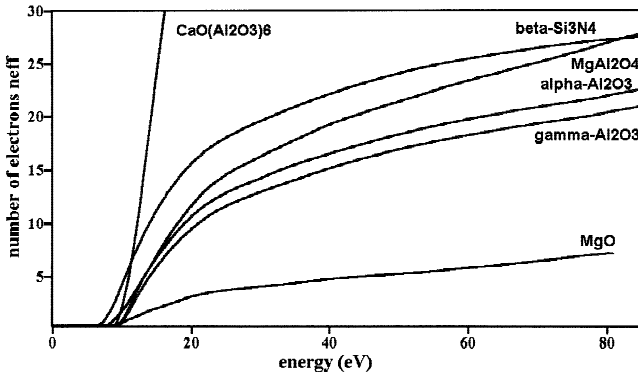
There is a well-known contribution from the surfaces to the VEEL spectrum. However, for the specimen thicknesses here, this was found to be insignificant. In the future, this will be corrected by the iterative procedure described by Egerton (1996). Similarly, the effect of a carbon coating applied to eliminate specimen charging could be removed by measuring the dielectric function of carbon in a separate experiment. Correction would require the thickness of the carbon film, which could be determined from the intensity of the C K-edge (Egerton, 1996).

The quantitative analysis also requires the refractive index of the material, but otherwise the analysis is fully self-contained. It is remarkable that the same quantitative values are obtained from fully independent methods such as VUV and VEEL spectroscopy (Müllejans and French, 1996; French et al., 1998a). The refractive index can be obtained from a handbook or determined by experimental methods (UV/VIS + ellipsometry). However, by just entering one value of the refractive index, the entire spectrum is provided by the analysis, i.e., the complex refractive index as a function of energy. According to Egerton (1996), the refractive index in the visible should be used rather than the static value. However, this is incorrect as the theoretical justification of the scaling is derived by setting  $E = 0$ . Therefore, the static value of the index of refraction should be used or, if it is measured, an extrapolation to zero energy has to be

**Table 1.** Materials Constants Used during Data Analysis

Material	$n$	$\rho$ (g/cm <sup>3</sup> )	V (nm <sup>3</sup> )	Z	Valence electrons	$n_{\text{eff}}$ (80 eV)	Exhausted transitions (%)
$\alpha$ -Al <sub>2</sub> O <sub>3</sub>	1.76	3.99	0.2547	6	24	22	92
$\gamma$ -Al <sub>2</sub> O <sub>3</sub>	1.70	3.56	0.0475	1	24	20.5	85
MgAl <sub>2</sub> O <sub>4</sub>	1.72	3.60	0.0656	1	32	21.5 <sup>a</sup>	67
MgO	1.73	3.58	0.07468	4	8	5.2 <sup>a</sup>	65
CaO(Al <sub>2</sub> O <sub>3</sub> ) <sub>6</sub>	1.8	3.785	0.586	2	152	117	77
$\beta$ -Si <sub>3</sub> N <sub>4</sub>	1.97	3.20	0.1456	2	32	27.3	85

<sup>a</sup>For MgO and MgAl<sub>2</sub>O<sub>4</sub>, the sum rule was evaluated up to 50 eV to exclude the Mg L-edge.

**Figure 3.** Sum rule for data of Figure 2.

made. In the present study, a value from the visible was used nevertheless, because the dispersion of the index of refraction between the visible and zero energy can be neglected for the large band gaps of the ceramic materials investigated (Loughin and French, 1998). For materials with smaller band gaps (semiconductors), more effort has to be put into the determination of the suitable index of refraction for the sum rule scaling.

Another way to consider the number of electrons involved in the valence interband transitions would be to evaluate the  $f$  sum rule using other optical properties such as the extinction coefficient  $k$  and the  $ELF$  (Smith, 1985; Egerton, 1996) [equations (3) and (4)]:

$$n_{\text{eff}}(E)|_k = \frac{m_0 v_f}{\pi^2 e^2 \hbar^2} \int_0^E E' k(E') dE'. \quad (3)$$

$$n_{\text{eff}}(E)|_{\varepsilon^{-1}} = \frac{m_0 v_f}{2\pi^2 e^2 \hbar^2} \int_0^E E' \text{Im} \left[ \frac{-1}{\varepsilon(E')} \right] dE'. \quad (4)$$

Equation (2) can be rewritten in a more common form (Shiles et al., 1980; Smith, 1985; Egerton, 1996) [equation (5)]:

$$n_{\text{eff}}(E)|_{\varepsilon} = \frac{m_0 v_f}{2\pi^2 e^2 \hbar^2} \int_0^E E' \varepsilon_2(E') dE'. \quad (5)$$

All three sum rules [equations (3–5)] have the same limiting value at high energy, but at intermediate energies they exhibit differing slopes and magnitudes. Therefore, they are sensitive to the accuracy and precision of the experimental data in differing energy regions and thus provide a means of checking the data for consistency.

One can evaluate these additional  $f$  sum rules up to an energy  $\hat{E}$ , which is defined as the energy at which valence transitions have been exhausted but the core level transitions have not yet started. The background dielectric constant  $\varepsilon_b$  of a fictitious medium consisting of only the polarizable atomic cores, without any valence electrons, can then be calculated (Shiles et al., 1980) [equation (6)]:

$$n_{\text{eff}}(\hat{E})|_{\varepsilon} = 2\sqrt{\varepsilon_b} n_{\text{eff}}(\hat{E})|_k = \varepsilon_b^2 n_{\text{eff}}(E)|_{\varepsilon}^{-1}. \quad (6)$$

$\varepsilon_b$  is the residual dielectric constant attributable to the core electrons that remain unexcited and we are currently implementing its determination.

Features in the interband transition strength can be directly related to the (calculated) electronic structure (French et al., 1988, 1994; Loughin, 1992; Loughin et al., 1993). Critical point modeling gives then detailed information about the type of the transitions (Loughin, 1992; Loughin et al., 1996). Sum rules applied to sub-sets of transitions provide the band occupancy and give an indication

of the type of bonding (Müllejjans and French, 1996). This has been applied originally to data where the interband transition strength was arbitrarily set to vanish above 44 eV. Our more recent analysis yields finite values of the interband transition strength up to much higher energies, which is demanded by the physics. For these data, the critical point modeling will have to be modified in the future. However, the qualitative results obtained previously in particular on the  $\Sigma_{11}$  grain boundary in alumina remain valid.

Together with the scan control described in the Materials and Methods section, it is possible to map the electronic structure in one (or two) dimensions. This has been utilized in the analysis of intergranular films in silicon nitride and the resulting forces (Hamaker constants) (Hamaker, 1937; French et al., 1995a, b, 1998b). This raises the question of the localization the VEEL spectrum (Howie 1981; Ritchie et al., 1990) and influences from interfaces (Howie and Milne, 1985). As is well known from dielectric theory, the VEEL spectrum measured with the primary electron beam near and parallel to an interface depends on the dielectric function of both media (Howie and Milne, 1985). This effect does not occur for grain boundaries where, by definition, the same material and, therefore, the same dielectric constant exists on both sides of the grain boundary. Therefore, a meaningful analysis of the changes in electronic structure at the grain boundary is feasible (Müllejjans and French, 1996). In the case of hetero-phase interfaces, however, account has to be taken of both bulk media (determined from separate measurements) before attempting to investigate the bonding at the interface. This application will only be addressable after extensive work.

The determination of the electronic structure from VEEL spectroscopy has a number of important advantages when compared to other methods. Compared with optical spectroscopy, a much higher spatial resolution is available, which allows investigation of interfaces and grain boundaries as well as materials, which cannot be made uniformly in large pieces. An example is silicon nitride, which always contains a certain percentage of intergranular glassy phases. The latter can be eliminated in the STEM by selecting a single grain but it always contributes in optical measurements. VEEL spectroscopy also extends to higher energy than optical spectroscopy. This could be overcome by employing synchrotron radiation as done by some groups (Hagemann et al., 1975; Tomiki et al., 1993). However, this is a rather expensive tool when compared to the VEEL spectroscopy in STEM, which is also somewhat more widespread and more easily accessible.

Naturally there are also drawbacks of the method, namely the inferior energy resolution when compared to optical spectroscopy and the inability to perform well-controlled experiments with polarized light. The former might be strongly alleviated by the introduction of monochromators currently under development which promise an energy resolution well below 1 eV [Rühle M, Mayer J (1999) SESAM project, private communication] and even down to 20 meV (Mook and Batson, 1999). The latter can be overcome by using synchrotron radiation (Tomiki et al., 1993). Optical spectroscopy has also been demonstrated at high temperatures (Bortz et al., 1990; French et al., 1988).

Obviously, no single method combines all advantages and therefore progress will only be made if the various techniques are regarded as complementary. Then each of them can be used to its specific potential. VEEL spectroscopy should play an important role in this context. For example, in the development of this analysis procedure, the comparison to results from VUV spectroscopy was invaluable. This allowed the optimization of many steps in the VEEL spectral analysis but also revealed limitations of the previous VUV analysis (see above discussion on critical point modeling) which were subsequently removed.

## CONCLUSIONS

---

Improved data acquisition and analysis methods for VEEL spectra provided the energy-loss function and its complex conjugate fully quantitatively for six different ceramic materials. From this, all other complex optical properties can easily be derived. The analysis of the interband transition strength gives access to the electronic structure and bonding of the material. This opens up a range of new applications, in particular the investigation of bonding at internal interfaces when combined with the high spatial resolution of a dedicated STEM. VEEL spectroscopy should be considered as an alternative and complementary method for determining optical properties and electronic structure of ceramic materials.

## ACKNOWLEDGMENTS

---

H.M. thanks Prof. Archie Howie for introducing him to the field of VEEL spectroscopy and its detailed analysis based on dielectric theory, and R.H.F. thanks Prof. Archie Howie for his support and encouragement in pursuing quantitative

VEEL analysis. We are indebted to Prof. M. Rühle for his continuous support and discussions. This work would not have been possible without the help of the STEM group at the Max-Planck-Institut für Metallforschung in Stuttgart over the years, in particular, Dr. G. Duscher for his excellent software and hardware development for data acquisition and A. Dorneich for detailed work on VEEL experiments and theory. We thank Dave Jones for his continuous help and Lin DeNoyer for development and constant improvement of electronic structure tools. We thank Drs. M. Čeh, W. Kaplan, I. Levin, M. Hoffman, and R. Schweinfest for provision of material and specimens. The technical work of M. Sycha in preparing TEM specimens and J. Thomas in maintaining the STEM was invaluable.

## REFERENCES

- Bortz ML, French RH (1989) Quantitative FFT-based, Kramers Kronig analysis for reflectance data. *Appl Spectrosc* 43:1498–1501
- Bortz ML, French RH, Jones DJ, Kasowski RV, Ohuchi FS (1990) Temperature dependence of the electronic structure of  $\text{Al}_2\text{O}_3$ ,  $\text{MgAl}_2\text{O}_4$  and  $\text{MgO}$ . *Phys Scripta* 41:537–541
- Ching WY (1990) Theoretical studies of the electronic properties of ceramic materials. *J Am Ceram Soc* 73:3135–3160
- Colliex C, Tencé M, Lefèvre E, Mory C, Gu H, Bouchet D, Jeanguillaume C (1994) Electron energy loss spectrometry mapping. *Mikrochim Acta* 114–115:71–87
- Craven AJ, MacKenzie M (1999) The use of ELNEs for microanalysis. In: *Microscopy and Microanalysis, Volume 5, Suppl. 2: Proceedings: Microscopy & Microanalysis '99, Portland, Oregon, August 1–5, 1999*, New York: Springer-Verlag, pp. 664–665
- Daniels J, Festenberg C, Raether H, Zeppenfeld K (1970) Optical constants of solids by electron spectroscopy. *Springer Tracts Mod Phys* 54:77–135
- Dorneich AD, French RH, Müllejans H, Loughin S, Rühle M (1998) Quantitative analysis of valence electron energy-loss spectra of aluminum nitride. *J Microsc* 191:286–296
- Echenique PM, Howie A, Wheatley DJ (1987) Excitation of dielectric spheres by external electron beams. *Philos Mag B* 56:335–349
- Egerton RF (1996) *Electron Energy-loss Spectroscopy in the Electron Microscope*, 2nd ed. New York: Plenum
- Fink J (1989) Recent developments in energy-loss spectroscopy. *Adv Electronics Electron Phys* 75:121–232
- French RH (1990a) Electronic band structure of  $\alpha\text{-Al}_2\text{O}_3$ , with comparison to  $\text{AlON}$  and  $\text{AlN}$ . *J Am Ceram Soc* 73:477–489
- French RH (1990b) Laser-plasma sourced, temperature dependent VUV spectrophotometer using dispersive analysis. *Phys Scripta* 41:404–408
- French RH, Coble RL, Kasowski RV, Ohuchi FS (1988) Vacuum ultraviolet photoemission and theoretical studies of the electronic structure of  $\text{Al}_2\text{O}_3$  up to 1000°C. *Physica B* 150:47–49
- French RH, Jones DJ, Loughin S (1994) Interband electronic structure of  $\alpha\text{-Al}_2\text{O}_3$  up to 2167 K. *J Am Ceram Soc* 77:412–422
- French RH, Cannon RM, DeNoyer LK, Chiang Y-M (1995a) Full spectral calculation of non-retarded Hamaker constants for ceramic systems from interband transition strengths. *Solid State Ion* 75:13–33
- French RH, Scheu C, Duscher G, Müllejans H, Hoffmann MJ, Cannon RM (1995b) Interfacial electronic structure and full spectral Hamaker constants of  $\text{Si}_3\text{N}_4$  intergranular films from VUV and SR-VEEL spectroscopy. In: *Proceedings of the Symposium on Structure and Properties of Interfaces in Ceramics*, Bonnell D, Chowdhry U, Rühle M (eds). Boston: Materials Research Society, 243–258
- French RH, Müllejans H, Jones DJ (1998a) Optical properties of aluminum oxide: determined from vacuum ultraviolet and electron energy-loss spectroscopies. *J Am Ceram Soc* 81:2549–2557
- French RH, Müllejans H, Jones DJ, Duscher G, Cannon RM, Rühle M (1998b) Dispersion forces and Hamaker constants for intergranular films in silicon nitride from spatially resolved-valence electron energy loss spectrum imaging. *Acta Mater* 46:2271–2287
- Galactic Industries (1996) *Grams/32*, 325 Main Street, Salem, NH 03079, USA
- Gatan Software E1/P v.3.0* (1994) Pleasanton, CA: Gatan Inc.
- Gautier M, Duraud JP, Le Gressus C (1987) Electronic structure of an  $\text{AlN}$  film produced by ion implantation, studied by electron spectroscopy. *J Appl Phys* 61:574–580
- Gorter CJ, Kronig R de L (1936) On the theory of absorption and dispersion in paramagnetic and dielectric media. *Physica III* 9:1009–1020
- Hagemann H-J, Gudat W, Kunz C (1975) Optical constants from the far infrared to the X-ray region: Mg, Al, Cu, Ag, Au, Bi, C and  $\text{Al}_2\text{O}_3$ . *J Opt Soc Am* 65:742–744
- Hamaker HC (1937) The London-Van der Waals attraction between spherical particles. *Physica* 4:1058–1072
- Howie A (1981) Localization and momentum transfer in inelastic scattering. In: *Proc EMSA 39th* Bailey GW (ed). pp 186–189
- Howie A, Milne RH (1985) Excitations at interfaces and small particles. *Ultramicroscopy* 18:427–434
- Howie A, Walsh CA (1991) Interpretation of valence loss spectra from composite media. *Microsc Microanal Microstruct* 2:171–181

- Johnson DW (1975) A Fourier series method for numerical Kramers-Kronig analysis. *J Phys A* 8:490–495
- Jones DJ, French RH, Müllejjans H, Loughin S, Dorneich AD, Carcia PF (1999) Optical properties of AlN determined by vacuum ultraviolet spectroscopy and spectroscopic ellipsometry data. *J Mater Res* 14:4337–4344
- Kramers HA (1927) La diffusion de la lumière par les atomes. *Atti Congr Intern Fis Como* 2:545–557
- Kronig R de L (1926) On the theory of dispersion of X-rays. *J Opt Soc Am* 12:547–557
- Levin I, Bendersky LA, Brandon DG, Rühle M (1997) Cubic to monoclinic phase transformations in alumina. *Acta Mater* 45:3659–3669
- Lide DR (ed) (1994) Physical constants of inorganic compounds. In: *Handbook of Chemistry and Physics, 74th Ed.* pp 4/36–4/114
- Loughin S (1992) *Vacuum Ultraviolet Spectroscopy and Analytical Critical Point Modeling of the Electronic Structure of Aluminum Nitride*. Dissertation, University of Pennsylvania
- Loughin S, French RH (1998) Aluminium nitride (AlN). In: *Handbook of Optical Constants of Solids III*, Palik ED (ed). New York: Academic Press, pp 373–401
- Loughin S, French RH, Ching WY, Xu YN, Slack GA (1993) Electronic structure of aluminum nitride: theory and experiment. *Appl Phys Lett* 63:1182–1184
- Loughin S, French RH, DeNoyer LK, Ching WY, Xu YN (1996) Critical point analysis of the interband transition strength of electrons. *J Phys D* 29:1740–1750
- Mo SD, Ching WY (1996) Electronic structure of normal, inverse, and partially inverse spinels in the MgAl<sub>2</sub>O<sub>4</sub> system. *Phys Rev B* 54:16555–16561
- Mook HW, Batson PE (1999) Integration of a monochromator in the field emission STEM. *Microsc Microanal* 5(Suppl 2):648–649
- Müllejjans H, French RH (1996) Interband electronic structure of a near  $\Sigma$ 11 grain boundary in  $\alpha$ -alumina determined by spatially resolved valence electron energy-loss spectroscopy. *J Phys D* 29:1751–1760
- Müllejjans H, Bruley J, French RH, Morris PA (1993) Quantitative electronic structure analysis of  $\alpha$ -Al<sub>2</sub>O<sub>3</sub> using spatially resolved valence electron energy-loss spectra. In: *Institute of Physics Conference Series 138, Electron Microscopy and Analysis Group '93, Liverpool, UK, 14–17 September 1993*, Craven AJ (ed). Bristol, UK: Institute of Physics, Pittsburgh, PA: Materials Research Society, pp 59–62
- Müllejjans H, Bruley J, French RH, Morris PA (1994) Quantitative electronic structure analysis of  $\alpha$ -Al<sub>2</sub>O<sub>3</sub> using spatially resolved valence electron energy-loss spectra. In: *Determining Nanoscale Physical Properties of Materials by Microscopy and Spectroscopy*, Boston, MA, November 29–December 3, 1993, Sarikaya M, Wickramasighe K, Isaacson M (ed). pp 169–176
- Müllejjans H, French RH, Duscher G, Rühle M (1997) Improved measurement and analysis of series of valence electron energy loss spectra and the local electronic structure. In: *Microscopy and Microanalysis, Volume 3, Suppl. 2: Proceedings: Microscopy & Microanalysis '97, Cleveland, Ohio, August 10–14, 1997*, New York: Springer-Verlag, pp 943–944
- Ritchie RH, Howie A (1977) Electron excitation and the optical potential in electron microscopy. *Philos Mag A* 36:463–481
- Ritchie RH, Howie A, Echenique PM, Besbas GJ, Ferrell FL, Ashley JC (1990) Plasmons in scanning transmission electron microscopy electron spectra. In: *Fundamental Electron and Ion Beam Interactions with Solids for Microscopy, Microanalysis and Microlithography*, Schou J, Kruit P, Newbury DE (eds). pp 45–56
- Ryen L, Wang X, Helmersson U, Olsson E (1999) Determination of the complex dielectric function of epitaxial SrTiO<sub>3</sub> films using transmission electron energy-loss spectroscopy. *J Appl Phys* 85:2828–2834
- Schweinfest R, Ernst F, Wagner T, Rühle M (1999) High-precision assessment of interface lattice offset by quantitative HRTEM. *J Microsc* 194:139–148
- Shiles E, Sasaki T, Inokuti M, Smith DY (1980) Self-consistency and sum-rule tests in Kramers-Kronig analysis of optical data: applications to aluminum. *Phys Rev B* 22:1612–1628
- Smith DY (1985) Dispersion theory, sum rules, and their application to the analysis of optical data. In: *Handbook of Optical Constants of Solids*, Palik ED (ed). New York: Academic Press, pp 35–68
- Spectrum Square Associates (1998) *Electronic Structure Tools*, 755 Snyder Hill Road, Ithaca, NY 14850, USA
- Tomiki T, Ganaha Y, Futemma T, Shikenbaru T, Aiura Y, Yuri M, Sato S, Fukutani H, Kato H, Miyahara T, Tamashiro J, Yonesu A (1993) Anisotropic optical spectra of  $\alpha$ -Al<sub>2</sub>O<sub>3</sub> single crystals in the vacuum ultraviolet region. II. Spectra of optical constants. *J Phys Soc Jpn* 62:1372–1387
- Walls MG (1987) *Electron Energy-loss Spectroscopy of Surfaces and Interfaces*. PhD thesis, University of Cambridge
- Walls MG, Howie A (1989) Dielectric theory of localized valence energy loss spectroscopy. *Ultramicroscopy* 28:40–42
- Walsh CA (1989) *Modeling and Interpretation of Electron Energy-loss Spectra from Interfaces*. PhD thesis, University of Cambridge
- Wooten F (1972) *Optical Properties of Solids*. New York: Academic Press
- Xu YN, Ching WY (1991) Self-consistent band structures, charge distributions, and optical-absorption spectra in MgO,  $\alpha$ -Al<sub>2</sub>O<sub>3</sub> and MgAl<sub>2</sub>O<sub>4</sub>. *Phys Rev B* 43:4461–4472
- Xu Y-N, Ching WY (1993) Electronic, optical, and structural properties of some wurtzite crystals. *Phys Rev B* 48:4335–4351